Proceedings of Engineering and Technology Innovation, vol. 29, 2025, pp. 26-46

Efficient Classification of Power Quality Using Long Short-Term Memory Network Technique

Mayyadah Sahib Ibrahim, Ali Sachit Kaittan*

Department of Electrical Power and Machines, College of Engineering, University of Diyala, Baqubah, Iraq

Received 08 June 2024; received in revised form 02 October 2024; accepted 04 October 2024

DOI: https://doi.org/10.46604/peti.2024.13831

Abstract

This study aims to apply a new deep-learning technique to detect and categorize individual and complex PQ issues such as swell, flickers, surges, interruptions, and sags. The suggested technique, the long short-term memory (LSTM) network, is a novel artificial intelligence technique and an identifiable form of recurrent neural network. This technique is utilized to detect and identify power quality (PQ) issues based on three principal solutions: automatic feature extraction, voltage/current magnitude calculations, and PQ problem duration. Simulated PQ problems generated by the Matlab simulation and many real field data sets are used to authorize the proposed technique's capability. The real data contain voltage and current waveforms that are measured, recorded, and analyzed in medium-voltage and high-voltage (MV/HV) substations by using a data acquisition device. The simulation results show that the proposed method is capable of detecting and classifying PQ problems more accurately compared with other artificial intelligence techniques.

Keywords: power quality, artificial intelligence, deep learning, LSTM

1. Introduction

The improvement of techniques for PQ disturbance classification has moved from conventional signal processing and statistical methods to more progressive machine learning and deep learning approaches. Among these, LSTM networks have emerged as a predominantly effective tool due to their ability to handle time-series data and the imprisonment of long-term dependencies. This emphasizes the need for continued research in the application and modification of deep learning models to further improve the accuracy and reliability of PQ disturbance classification [1].Power quality (PQ) problems refer to any fluctuations in current, voltage, or frequency, such as harmonic distortion, swells, interruptions, sags, flickers, and surges. Unexpected changes in current or voltage from their normal state can interrupt or damage any electrical equipment installed for critical functions within the electric power system.

Most domestic, commercial, and industrial electrical systems have non-linear loads, which inject more harmonics into the electric power systems, increasing voltage and current distortion and reducing overall power quality [2].Over the past several years, a substantial amount of research on power quality (PQ) has been published, focusing on various methods for analyzing and detecting PQ problems. Khetarpal et al. [3] utilized the Fourier transform (FT) in computational algorithms for analyzing stationary signals by extracting the spectrum at several specified frequencies. This analysis allows the signal to be viewed as an aggregate of sine waves of different frequencies. Cen et al. [4] detected the presence of a component with a specific frequency in the signal, even in the absence of any data at the time when that frequency component becomes prominent. Consequently, time information is often neglected during the transformation of the signal to the frequency domain.

* Corresponding author. alisachit@uodiyala.edu.iq

English language proofreader: Si-Yu Lin

The short-time Fourier transform (STFT) method has been used to classify and identify power quality (PQ) problems in the time-frequency domain, as presented in [5]. However, the STFT is suitable only for stationary signals where frequency does not vary with time. For signals in a non-stationary state, the STFT fails to identify the dynamic properties of the signal due to the limited width of the fixed window. Wavelet transform (WT) methods have been employed to extract information on time and frequency for PQ problems, as reported in [6]. As a well-regarded and effective approach to feature representation in the time-frequency domain, WT offers improved support for signal analysis. However, the disadvantages of WT include complex calculations and sensitivity to noise levels.

The s-transform (ST) has been documented as an efficient method for processing PQ signal problems. It builds upon the conceptions of the short-time Fourier transform (STFT) and wavelet transform (WT), offering definite advantages over both methods. The ST preserves high-frequency resolution, allowing for the detection of high-frequency transients and providing good frequency resolution over long periods. Several studies have used the ST technique for the detection and classification of power quality (PQ) problems [7-8].

The Hilbert-Huang transform (HHT) has been acknowledged as a highly suitable method for detecting instantaneous events in non-stationary and non-linear PQ problems. The HHT technique can efficiently detect instantaneous events in various PQ problems, even under noisy circumstances [9]. The discrete Gabor transform (DGT) is an improved form of the STFT, as noted in [10]. The input signal in the DGT is focused around a window function and transformed using the FT to simplify time-frequency analysis. The main benefits of the DGT include a smaller feature size, reduced execution time, and greater accuracy. Consequently, the DGT technique requires low memory usage during both testing and training procedures. The modification of the basic component amplitude of the voltage source using the Kalman filter (KF) to analyze and detect voltage events was first presented in [11]. The KF outcomes depend on the system model and the suitable choice of filter parameters [12].

By integrating AI and signal processing techniques into a hybrid model, it is possible to provide the strengths of both approaches. This combined use raises the accuracy, robustness, and interpretability of power quality (PQ) synthesis systems, resulting in more effective and reliable performance, particularly in real-world and real-time applications [13]. Future research could investigate developing adaptive algorithms that dynamically balance the computational load between AI and signal processing mechanisms, further optimizing performance [14-17].

This study presents a design for an optimal aggregation of a hybrid solar-wind turbine and battery bank setup model, examining the potential for energy generation to meet domestic load demand. Long-term time series data on wind speed and solar radiation were collected to evaluate the wind and solar power potential in Zurbatiyah Subdistrict, Badra District, Wasit Governorate, Iraq. Wind speed data were analyzed using Windographer software, while solar radiation data were analyzed with PVsyst 7.1 software to assess the solar energy potential and photovoltaic system performance. The expected energy production from the hybrid system, which involves a 4.0 kW small wind turbine and a 4.0 kW solar photovoltaic scheme, aims to fulfill the local residential electricity needs.

The rest of the study is organized as follows: Section 2 presents the suggested technique using the LSTM network. Section 3 demonstrates the simulation results, while Section 4 describes the practical results. Section 5 discusses these results, and the conclusions of this work are presented in Section 6.

2. Proposed Technique

The proposed technique is the long short-term memory (LSTM) method, which is a specific case of recurrent neural network (RNN) used for automatically learning properties, identifying, discovering, and classifying power quality (PQ) events and problems.

2.1. Background

LSTM is a type of recurrent neural network (RNN) capable of learning long-term dependencies. It can encode time series problems over both long and short durations using a memory cell (hidden layer). LSTM is specifically designed to overcome the vanishing gradient problem that RNNs often encounter by maintaining a constant error that can propagate through the network over time.

(1) LSTM network architecture: The LSTM architecture consists of a series of cells, arranged as three layers

I Input layer: Receives the input data sequence.

II Hidden layers: The core of the LSTM network, which includes three main gates that regulate the flow of information:

(I) forget gate: Decides what information from the previous cell state should be discarded.

(II) input gate: Determines which new information should be stored in the cell state.

(III) output gate: Determines the output of the current cell and what information should be passed to the next cell.

III Output layer: Produces the final classification or prediction.

A detailed diagram is shown in Fig. 1 [18].

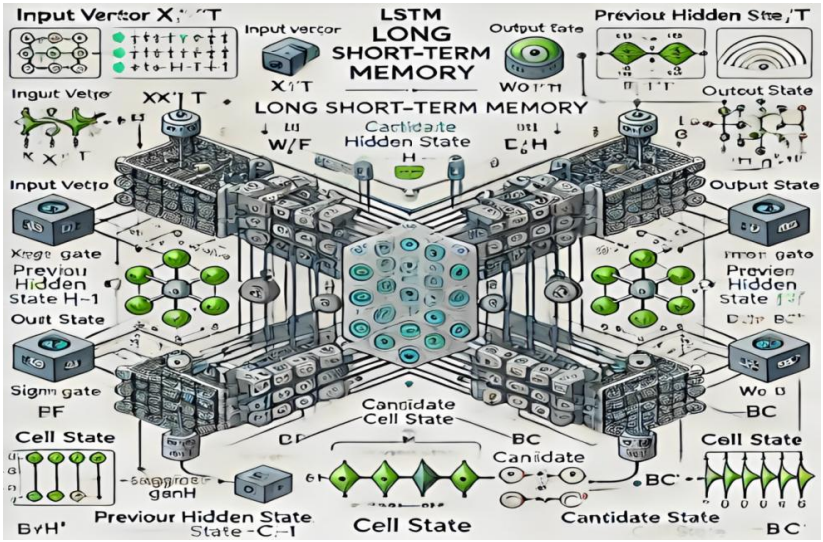

Fig. 1 Architecture of LSTM network system

(2) Recurrent neural networks (RNNs): RNNs contain a loop in the interior networks to ensure the persistence of information. RNNs are fully connected layers as well as among the nodes within the same layers. In addition, hidden cells in RNNs receive feedback from the previous states to the current state [19]. Fig. 2 shows the construction of the LSTM network, with a layer of sequence input at the start, a layer of LSTM, and a layer of prediction at the end.

Fig. 2 Construction of LSTM network system

The principle behind LSTM architecture is a memory cell, which can maintain its status for a definite time. The non-linear mechanism of this cell can regulate the data flow in/out of the cell of the LSTM. The LSTM networks are used to develop a deeper neural network that is nonlinear. The hidden layer is constructed to contain a memory cell, which includes an input gate, a forget gate, an output gate, and a recurrent connection unit.

(3) LSTM Layer construction: Fig. 3 shows the inflow of time-series data (X) with a time step (t) through the LSTM layer. The layer state includes the cell state (c) and the hidden state (h). At time step (t), the hidden state includes the layer of LSTM output at this step [20].

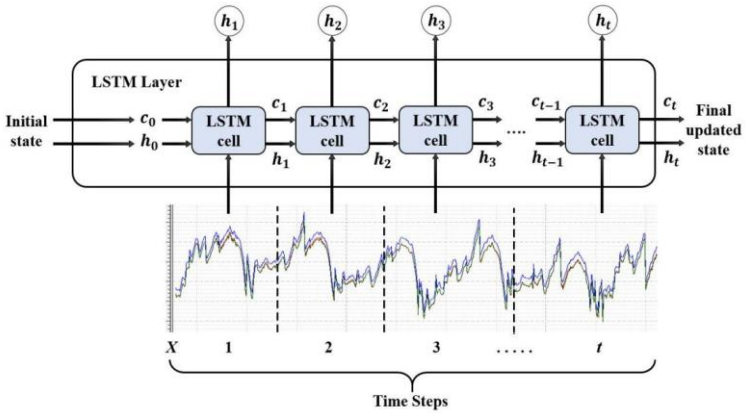

Fig. 3 LSTM layer with a flow of time series data

The cell state includes all data acquired from the preceding steps. At each time step, the LSTM layer eliminates or adds data to the cell state. According to this operation, the LSTM layer uses gates to control the cell updates as shown in Table 1.

Table 1 Cell state and hidden state control gates

Gate	Objective
Input (i)	Update the cell state
Forget (f)	Reset the cell state
Layer input (g)	Insert data into the cell state
Output (o)	Add cell state to the output state

The primary LSTM cell takes the initial case of the network and the initial time step (x1) and calculates the initial output (h1) and the cell state (c1). At time step (t), the LSTM cell takes the network's previous state (ct−1, ht−1) and the next input (xt) to calculate the output state (ht) and the updated cell state (ct). Fig. 4 presents the structure of the LSTM cell and the function of the gates for updating the hidden and the cell states [21].

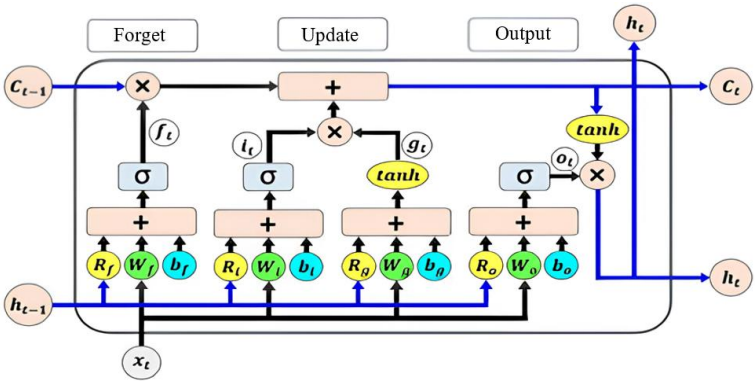

Fig. 4 Structure of LSTM cell

As presented in Eq. (1), the matrices *W*, *R*, and *b* represent the input and recurrent weights, and the bias for each component, respectively.

$$W = \begin{bmatrix} W_i \\ W_f \\ W_g \\ W_o \end{bmatrix}, R = \begin{bmatrix} R_i \\ R_f \\ R_g \\ R_o \end{bmatrix}, b = \begin{bmatrix} b_i \\ b_i \\ b_g \\ b_o \end{bmatrix} \tag{1}$$

where the i, f, g, and o represent the input, forget, LSTM layer input, and the output gates, respectively.

Table 2 Formula for each gate at time step (t)

Gate	Formula
Input (*i*)	$i_t = \sigma(W_i x_t + R_i h_{t-1} + b_i)$
Forget (*f*)	$f_t = \sigma(W_f x_t + R_f h_{t-1} + b_f)$
Layer input (*g*)	$g_t = \tanh(W_g x_t + R_g h_{t-1} + b_g)$
Output (*o*)	$o_t = \sigma(W_o x_t + R_o h_{t-1} + b_o)$

The tanh function changes all cell states, but the gates use a sigmoid function (σ), which is used for transformation and prediction in neural networks. The LSTM cell is defined by the following equations, for each component at time step (t), as shown in Table 2.

$$\sigma(x) = \frac{1}{(1+e^{-x})} \tag{2}$$

$$c_t = f_t \odot c_{t-1} + i_t \odot g_t \tag{3}$$

where it is the state of a cell at the time (t), and $\odot$ is element-wise vector multiplication. The hidden state at the time (t) is given by [22]:

$$h_t = o_t \odot \tanh(c_t) \tag{4}$$

2.2. Noise analysis and mitigation techniques

Various signal-to-noise ratios (SNRs) are considered to understand the model's robustness in practical environments. Noise can significantly affect the accuracy of detection by presenting variability and uncertainty in the input data. To address this, the model compensates for noise using regularization techniques, data augmentation, and noise filtering during preprocessing. Furthermore, the LSTM network's architecture is optimized to learn robust patterns even in noisy conditions.

2.3. Hyperparameter optimization

The hyperparameters of the LSTM network, including the number of hidden layers, learning rate, batch size, and number of epochs, are selected and optimized using grid search and cross-validation techniques. Various configurations are experimented with to determine the optimal settings that maximize model performance while preventing overfitting. The final configuration used for the experiments includes the accuracy and loss metrics.

2.4. Implementation

The LSTM method is designed to implement the identification and discovery process using four parameters: amplitude, start time, end time, and problem period, and one output for the waveform class as shown in Fig. 5.

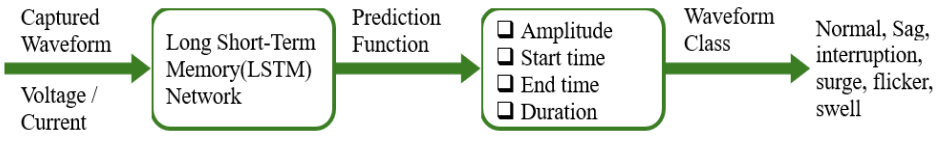

Fig. 5 Construction of the proposed technique

The set of PQ problems includes surge, normal, flicker, sag, interruption, and swell. Any output that does not belong to these categories is considered a distortion. The LSTM system output can take values as shown in Table 3.

Table 3 LSTM system output values

PQ disturbance	LSTM network output
Interruption signal	0
Sag signal	0.5
Normal sine wave signal	1
Swell signal	1.5
Surge signal	3

The datasets used for training and testing consist of (describe the datasets' size, diversity, and origin). These datasets include a range of PQ disturbances such as voltage sags, swells, transients, harmonics, and interruptions, collected from (specify the source, e.g., simulated environments, real-world power grids). To ensure adequate representation of different PQ issues, the data are augmented using techniques such as noise injection, scaling, and time-shifting.

The plain text of pseudocode for LSTM Implementation can be written as follows:

(1) Initialize network parameters: Input size, Hidden size, Output size, Learning rate, and Number of epochs.

(2) For each training epoch:

I For each input sequence x_t:

(I) Compute the forget gate: $f_t = \sigma(W_f x_t + R_f h_{t-1} + b_f)$

(II) Compute the input gate: $i_t = \sigma(W_i x_t + R_i h_{t-1} + b_i)$

(III) Compute the candidate cell state: $g_t = \tanh(W_g x_t + R_g h_{t-1} + b_g)$

(IV) Update the cell state: $c_t = f_t \odot c_{t-1} + i_t \odot g_t$

(V) Compute the output gate: $o_t = \sigma(W_o x_t + R_o h_{t-1} + b_o)$

(VI) Update the hidden state: $h_t = o_t \odot \tanh(c_t)$

(3) Compute the loss and backpropagate the error to update weights and biases.

(4) Repeat until convergence or until the maximum number of epochs is reached.

3. Simulation results

The signals simulating the power quality (PQ) problems are generated by a MATLAB program using a mathematical model, as shown in Table 4 [23-24]. Each simulated waveform is sampled at a rate of 3.2 kHz (64 samples per cycle).

Table 4 Mathematical models of PQ problems

PQ problem	mathematical model	technical parameters
pure wave signal	$V(t) = A\sin(\omega t)$	$\omega = 2\pi f$
sag signal	$V(t) = (1-\alpha(u(t-t_1)-u(t-t_2)))\sin(\omega t)$	$0.1 \le \alpha \le 0.9$, $T \le t_2 - t_1 \le 9T$
swell signal	$V(t) = (1+\alpha(u(t-t_1)-u(t-t_2)))\sin(\omega t)$	$0.1 \le \alpha \le 0.8$, $T \le t_2 - t_1 \le 9T$
interruption signal	$V(t) = (1-\alpha(u(t-t_1)-u(t-t_2)))\sin(\omega t)$	$0.9 \le \alpha \le 1$, $T \le t_2 - t_1 \le 9T$
surge signal	$V(t) = \sin(\omega t) + \alpha e^{-(t-t_1)/T}(u(t-t_1)-u(t-t_2))\sin(\omega t)$	$1.8 \le \alpha$, $T \le t_2 - t_1 \le 9T$
flicker signal	$V(t) = (1+\alpha f \sin(\beta\omega t))\sin(\omega t)$	$0.1 \le \alpha f \le 0.2$, $5 \le \beta \le 20Hz$
harmonic signal	$V(t) = \alpha_1\sin(\omega t) + \alpha_3\sin(3\omega t) + \alpha_5\sin(5\omega t) + \alpha_7\sin(7\omega t)$	$0.1 \le \alpha_3, \alpha_5, \alpha_7 \le 0.15$, $\sum \alpha_i^2 = 1$

While MATLAB provides a powerful environment for modeling and simulating power systems, certain practical details such as real-world noise, component aging, environmental variations, and unexpected operational conditions may not be fully captured in a simulation environment. Several assumptions were made to simplify the modeling process, including ideal

operating conditions, linear system components, and controlled data input. For the types of PQ events and problems, one hundred training events are executed by changing the start time, the magnitude of the amplitude, and the ending time of each and every PQ disturbance and problem. Most simulated signals are merged with different signal-to-noise ratio (SNR) values, including 40 dB, 30 dB, and 20 dB.

As shown in Eq. (5), SNR is the ratio of signal power to noise power, expressed in decibels(dB). An SNR with a ratio greater than 1:1 (0 dB) indicates that the signal is stronger than the noise.

$$SNR = \frac{p_{signal}}{p_{noise}} \tag{5}$$

A high SNR indicates better design and more suitable data and evidence than undesirable data.

In addition to accuracy, other evaluation metrics such as precision, recall, and the F1-score are included to provide a more comprehensive assessment of the model's performance. Precision measures the proportion of correctly identified positive instances out of all instances predicted as positive, while recall assesses the model's ability to correctly identify all relevant instances. The F1-score, a harmonic mean of precision and recall, provides an overall metric that balances both concerns. These metrics help illustrate the model's effectiveness in correctly identifying various types of PQ disturbances [25].

3.1. Voltage interruption

The voltage interruption is the complete loss of voltage, dropping below 0.1 p.u., on one or more phases for a definite period. The simulated interruption waveform mixed with SNR 40 dB is shown in Fig. 6(a). The amplitude magnitude and the output of the LSTM technique for this signal are displayed in Figs. 6(b) and 6(c), respectively. The LSTM output equals zero, indicating that this signal represents an interruption waveform.

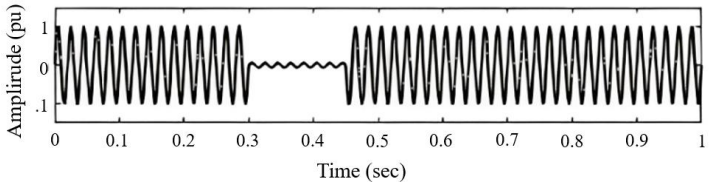

(a) Waveform

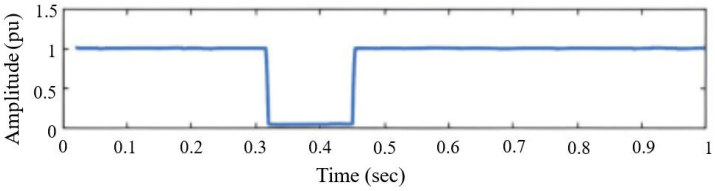

(b) Magnitude

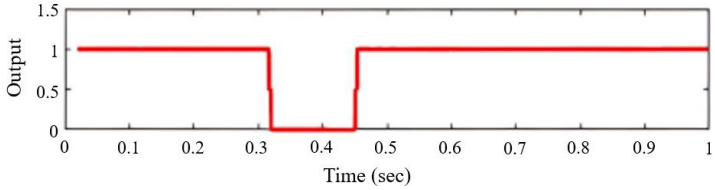

(c) LSTM output

Fig. 6 Voltage interruption with SNR 40 dB

3.2. Voltage sag

The sag signal is a sudden reduction in RMS voltage amplitude, typically between 0.1-0.9 p.u., followed by the voltage recovery after a period of duration time from a few cycles to a few seconds. The voltage sags are caused by the electrical short circuit, switching of large loads, and power fluctuations of speed drives. The simulated sag waveform is mixed with the SNR

of 30 dB which is shown in Fig. 7(a). The magnitude or amplitude and the output of the LSTM technique of this signal are shown in Figs. 7(b) and 7(c), respectively. The output of LSTM equals 0.5, this means that this waveform is a voltage sag waveform.

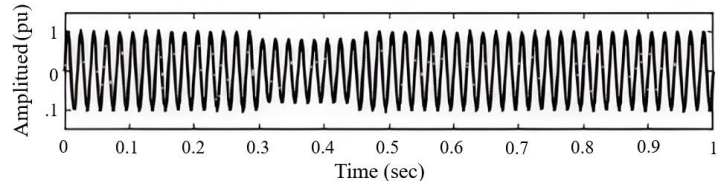

(a) Waveform

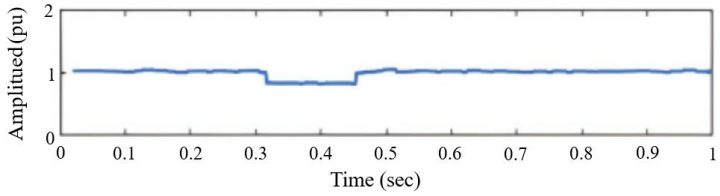

(b) Magnitude

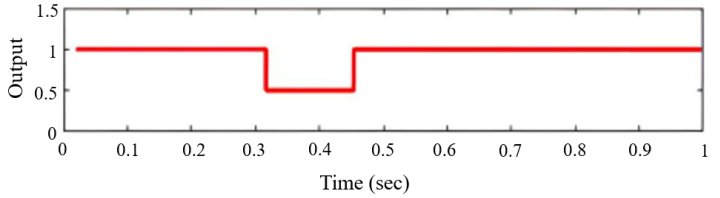

(c) LSTM output

Fig. 7 Voltage sag with SNR 30 dB

3.3. Voltage distortion

Voltage distortion occurs when sinusoidal voltages contain multiple frequencies in addition to the fundamental power system frequency. This distortion is caused by using nonlinear loads. The simulated voltage distortion waveform mixed with the SNR of 30 dB is shown in Fig. 8(a). The magnitude and the output of the LSTM method for this signal are shown in Figs. 8(b) and 8(c), respectively. The LSTM output equals 1, indicating that this is a distorted waveform.

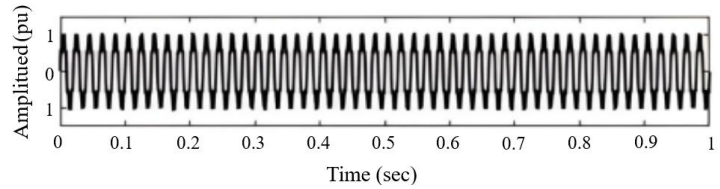

(a) Waveform

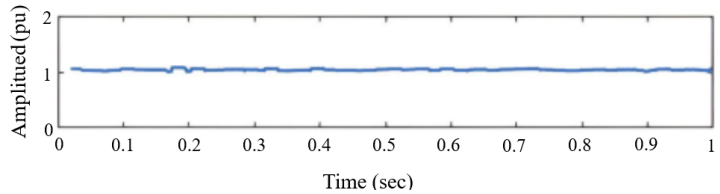

(b) Magnitude

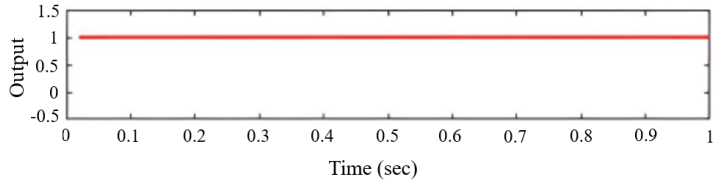

(c) LSTM output

Fig. 8 Voltage distortion with SNR 30 dB

3.4. Voltage swell

Voltage swell is a temporary increase, between 1.1-1.8 p.u., in the RMS voltage magnitude of the healthy phases when an earth fault occurs in one of the phases for a short period of time ranging from 0.5 cycles to 1 minute. The voltage swell is caused by the disconnection of large loads. The simulated voltage swell waveform is mixed with the SNR of 20 dB and is shown in Fig. 9(a). The magnitude and the LSTM output for this signal are shown in Figs. 9(b) and 9(c), respectively. The output of the LSTM equals 1.5, meaning that this is a voltage-swell waveform.

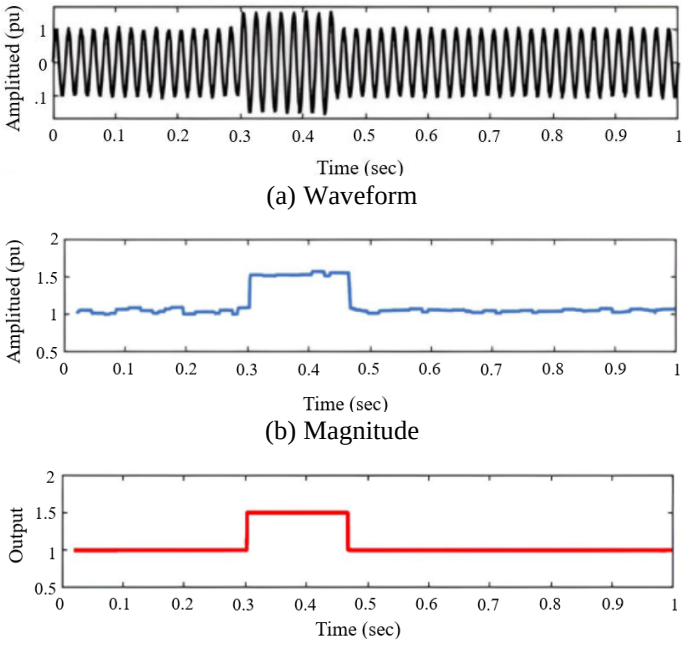

Fig. 9 Voltage swell with SNR 20 dB

3.5. Voltage surge

The voltage surge is a sudden increase in RMS voltage magnitude, between 1-3 p.u., lasting for a short duration of time of only a few cycles. Voltage surges occur due to the disconnection of the heavy loads. The simulated voltage surge waveform is mixed with the SNR of 30 dB and is shown in Fig. 10(a). The magnitude and the LSTM output for this waveform are shown in Figs. 10(b) and (c), respectively. The output of the LSTM equals 3, this means that this waveform is a surge waveform.

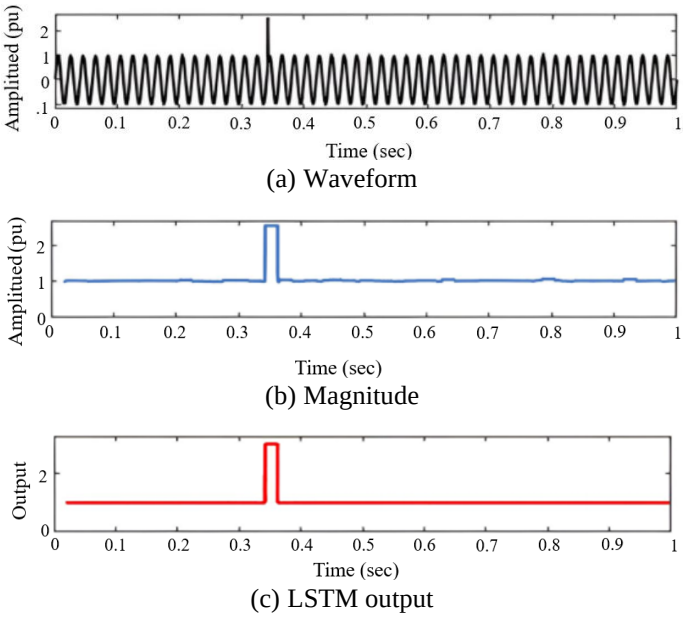

Fig. 10 Voltage surge with SNR 30 dB

3.6. Voltage flicker

Voltage flicker is a rapid change in RMS voltage magnitude, typically between 0.9-1.1 p.u. Flicker results from the visible voltage fluctuations in lamps and is caused by arc furnaces. The simulated voltage flicker signal, the magnitude, and the LSTM technique output are shown in Figs. 11(a), (b), and (c) respectively.

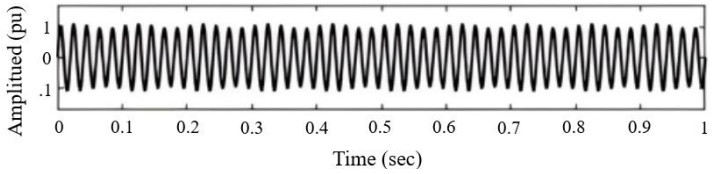

(a) Waveform

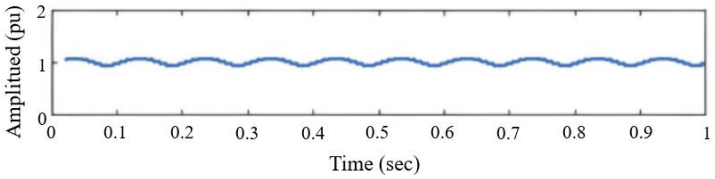

(b) Magnitude

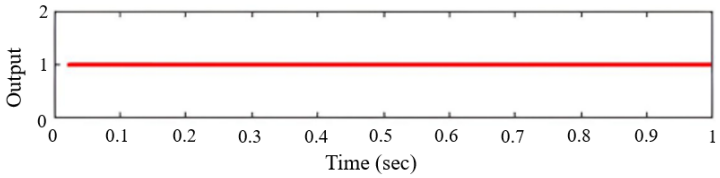

(c) LSTM output

Fig. 11 Voltage flicker

3.7. Comparative analysis

To confirm the LSTM method efficiency, its prediction results are compared with the other AI techniques results, such as Kalman filter and fuzzy-expert system (KF, FES) [12], adaptive linear neuron (ADALINE), feed-forward neural networks (FFNN) [26], s-transform and dynamics (ST and dynamics) [27-28], double resolution s-transform (DRST), directed acyclic graph (DAG) [29], sparse signal decomposition on hybrid dictionaries (SSD on hybrid dict.), and fuzzy decision tree (fuzzy DT) [30].

Table 5 Comparison of several prediction techniques for noiseless PQ disturbances and problems

	Noiseless			
	ADALINE and FFNN [26]	DRST, DAG [27]	SSD on hybrid dict. [30]	Proposed LSTM network
Normal	100.0	100.0	100.0	100.0
Interruption	100.0	97.0	100.0	100.0
Sag	100.0	99.5	100.0	100.0
Flicker	94.0	99.5	100.0	100.0
Swell	100.0	99.0	100.0	100.0
Surges	-	-	-	100.0
Harmonics	98.0	100.0	100.0	100.0
Sag with Harmonics	98.0	100.0	84.67	100.0
Swell with Harmonics	97.0	99.5	86.0	100.0
Mean (%)	98.38	99.31	96.33	100.00

The LSTM technique is evaluated both with and without high-noise conditions. Statistical significance tests, such as p-values, are used to assess the differences in performance metrics (accuracy, precision, recall, F1-score) across various datasets. All p-values obtained are below 0.05, indicating that the LSTM model's developed performance is statistically significant. The results establish the superiority of the LSTM approach in handling complex, time-dependent patterns in power-quality data. The total results and the categorization accuracies for noiseless and noisy states and conditions at 20 dB, 30 dB, and 40 dB are 100%, 94.56%, 98.22%, and 99.94%, respectively which are summarized in Tables 5-8.

Table 6 Comparison of several prediction techniques for different PQ disturbances and problems with 20 dB SNR

PQ disturbance	With 20 dB SNR				
	KF, FES [12]	ST and dynamics [28]	ADALINE, FFNN [26]	DRST, DAG [30]	Proposed LSTM network
Normal	-	96.0	90.0	100.0	97.0
Interruption	92.0	85.0	100.0	92.0	94.0
Sag	93.0	95.0	98.0	99.0	95.0
Flicker	-	91.0	87.0	97.0	93.0
Swell	94.0	97.0	99.0	98.5	94.0
Surges	92.0	-	-	-	95.0
Harmonics	90.0	97.0	90.0	99.5	94.0
Sag with Harmonics	93.0	95.0	89.0	99.5	95.0
Swell with Harmonics	92.0	97.0	88.0	97.0	94.0
Mean (%)	92.29	94.13	92.63	97.81	94.56

Table 7 Comparison of several prediction techniques for different PQ disturbances and problems with 30 dB SNR

PQ disturbance	With 30 dB SNR				
	ST and fuzzy DT [27]	KF, FES [12]	ST and dynamics [28]	SSD on hybrid dict. [30]	Proposed LSTM network
Normal	-	-	100.0	100.0	99.0
Interruption	96.67	98.0	96.0	98.0	97.5
Sag	97.33	99.0	99.0	100.0	99.0
Flicker	-	-	96.0	100.0	98.0
Swell	98.67	99.0	98.0	100.0	99.0
Surges	-	96.0	-	-	98.0
Harmonics	100.0	94.0	99.0	100.0	98.0
Sag with Harmonics	-	97.0	97.0	83.33	98.0
Swell with Harmonics	96.0	96.0	98.0	82.67	97.5
Mean (%)	97.73	97.00	97.88	95.50	98.22

Table 8 Comparison of several prediction techniques for different PQ disturbances and problems with 40 dB SNR

PQ disturbance	With 40 dB SNR				
	ST and fuzzy DT [27]	KF, FES [12]	ST and dynamics [28]	SSD on hybrid dict. [30]	Proposed LSTM network
Normal	-	-	100.0	100.0	100.0
Interruption	96.67	100.0	98.0	100.0	99.5
Sag	97.33	100.0	100.0	100.0	100.0
Flicker	-	-	98.0	100.0	100.0
Swell	98.67	100.0	100.0	100.0	100.0
Surges	-	98.0	-	-	100.0
Harmonics	100.0	97.0	100.0	100.0	100.0
Sag with Harmonics	-	98.0	99.0	84.67	100.0
Swell with Harmonics	98.0	98.0	99.0	86.0	100.0
Mean (%)	98.13	98.71	99.25	96.33	99.94

4. Practical Results

This section presents some of the practical and real output results to ensure the LSTM technique's ability to discover and categorize PQ problems. Before reviewing the practical results, it is important to introduce certain concepts and the tool settings used to achieve these results. Therefore, we must delve into these concepts, the challenges that hinder the application of the proposed method, and how to deal with them.

4.1. Field data setup

The measurements of the field and the site are taken from the secondary power transformer side of rating 25MVA - 66/11KV and the transformers supply the electric power to different loads including industrial, residential, and commercial. A part of the single-line diagram (SLD) and measurement location of the acquisition device is shown in Fig. 12.

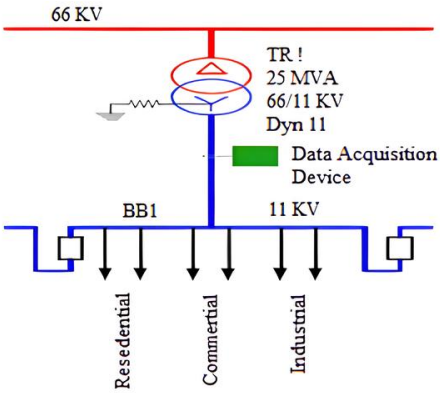

Fig. 12 Part of SLD of HV substation with data ACQ device location

4.2. Data acquisition device

The data acquisition (DAQ) device is a great performing, power-analyzing equipment, and event recording device. Data DAQ device applies the IEC 61000-4-30 specification for voltage detection and measurements, enabling it to identify, calculate

the period of time, and measure all events values related to harmonic distortions, inter-harmonics, voltage asymmetry, frequencies, flickers, and time synchronizations. These measurements are performed using the connections shown in Figs. 13(a) and (b). Through each second, the DAQ equipment records multiple data on phase and line currents, voltages, active and reactive power, harmonic distortions, power factors, and power system frequency. The recorded data and outputs give an in-depth overview of the total performance of the proposed method. The sampling frequency (fs) used in the DAQ device is 41 KHz or 820 sample/cycle at a frequency of 50 Hz.

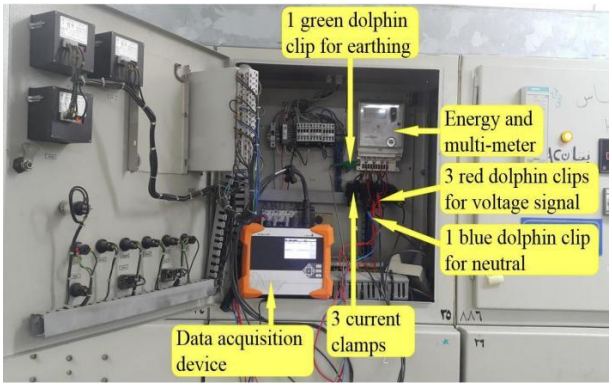

(a) Practical and site connection of data DAQ device

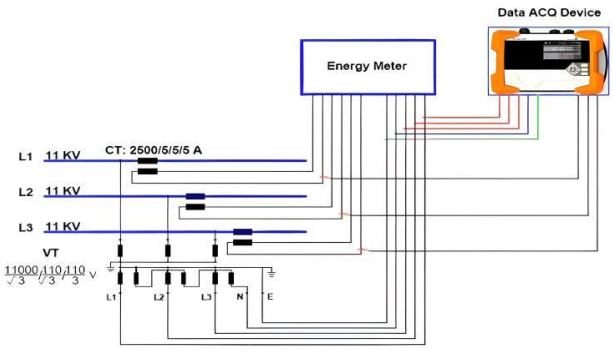

(b) SLD of data DAQ device connection with the secondary core of CT and PT

Fig. 13 Installation of data DAQ device

4.3. Practical application limitations and scalability considerations

The proposed method's scalability is tested by gradually increasing the dataset size and input sequence length. While LSTM networks are integrally computationally intensive, the use of the DAQ device significantly reduces the processing time and latency by optimizing real-time data acquisition and transmission. Future research will explore additional optimizations and the application of lightweight models for deployment in resource-constrained environments. The DAQ device is enhanced to lessen processing time and potential issues by using advanced digital signal processing (DSP) techniques to pre-process the data before it is fed into the LSTM network.

This pre-processing step decreases the data size and complexity, allowing the LSTM network to focus on critical structures, which in turn reduces the time required for model inference. Furthermore, the DAQ device is equipped with high-speed communication interfaces that guarantee rapid data transfer, further decreasing latency. The DAQ device is specifically designed to handle continuous data streams efficiently. It uses a buffer management system that ensures data is collected and transferred in real-time without interruptions or data loss. This capability, combined with the LSTM network's construction, allows the system to process data continuously and provide timely predictions and classifications of power quality issues.

5. Results and Discussions

The results of this study provide real-world validation of the proposed LSTM-based approach for power quality (PQ) analysis. By using real data from an HV/MV substation, the system establishes its effectiveness in classifying and categorizing numerous PQ problems, such as interruptions, voltage sags, swells, and harmonic distortion. Additionally, several key concepts must be considered in achieving these results, as listed below.

5.1. Assumptions and limitations

In this study, several assumptions were made to simplify the modeling and analysis procedure. Firstly, the data used for training and validation are assumed to be demonstrative of typical power quality (PQ) disturbances, but they may not cover all possible real-world scenarios. Additionally, ideal operating conditions are assumed, such as steady environmental factors and

fully functional components. Furthermore, the model relies on the availability of high-quality datasets, which may not always be approachable or may vary considerably in real-world applications. These assumptions may bind the generality of the proposed methodology to all possible PQ problems. Future work should focus on validating the model under more diverse and challenging conditions, including various noise levels, diverse grid configurations, and dynamic operational environments.

5.2. Validation with real-world data

Although this study provides an initial assessment using simulated data, additional testing with real-world datasets is essential to confirm the model's robustness and practical applicability. Future work will involve collaboration with industry partners to obtain high-quality, real-world data and validate the model under different operating conditions. Preliminary results from initial real-world testing have shown promising arrangement with the simulated data results, suggesting the model's latent for effective deployment in practical situations.

5.3. Model interpretability

To improve the interpretability of the LSTM model's decision-making process, techniques such as attention mechanisms and feature importance analysis, have been employed. The attention mechanism allows the model to focus on specific parts of the input sequence that are most applicable to the forecasting, while feature importance analysis classifies which features contribute most to the model's decisions. These approaches provide insights into the model's internal workings, making it more transparent and reliable for practical applications.

5.4. Error analysis

To better understand the limitations of the projected LSTM model, a detailed error analysis has been accompanied. This analysis examined cases where the model misclassified PQ disturbances, detecting common patterns among the errors. The results indicate that most misclassifications happened with disturbances that have overlapping characteristics, such as differentiating between certain sorts of harmonics and voltage sags. These errors could be attributed to insufficient diversity in the feature space for similar disturbances. Future enhancements will focus on improving feature extraction and refining the model to better distinguish between closely associated PQ problems.

5.5. Training accuracy and loss curves

To demonstrate the model's learning process and convergence behavior over time, training accuracy and loss curves are plotted in Fig. 14 and Fig. 15, respectively. The curves show that the LSTM model converges steadily, with both the training accuracy increasing and the loss decreasing steadily over the epochs. The curves confirm that the model is neither overfitting nor underfitting, which is crucial for its robustness and generalizability in practical applications.

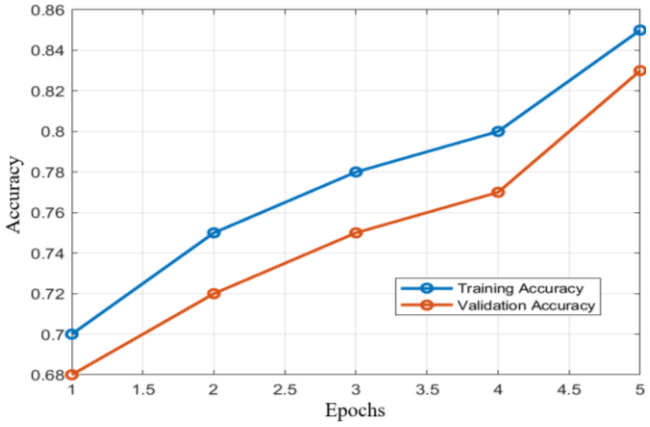

Fig. 14 Training and validation accuracy

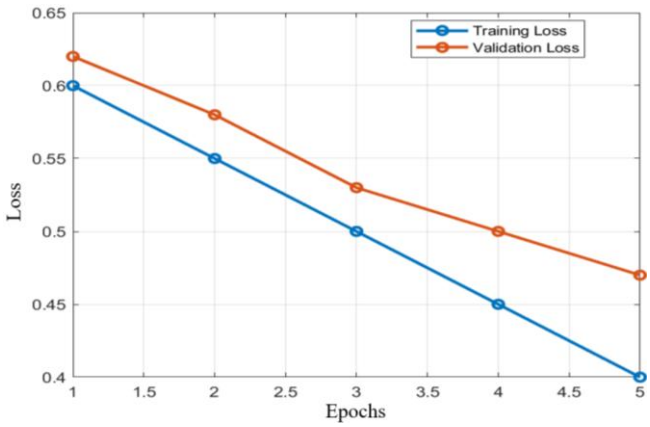

Fig. 15 Training and validation loss

The model shows steady improvement in both training and validation accuracy across epochs, with minimal overfitting. By the fifth epoch, the model achieves a high training accuracy of 85% and a solid validation accuracy of 83%, indicating good generalization. However, there is still potential for improving validation performance, possibly through additional training or fine-tuning of hyperparameters. Both training and validation loss steadily decrease over the five epochs, indicating that the model is learning effectively.

The gap between training and validation loss remains small, suggesting minimal overfitting. The reduction in loss reflects the model's improved ability to predict accurately as the training progresses. Further tuning may heighten performance, but these results already show solid convergence.

5.6. Recorded data 1 (*recorded data are for 3ph voltages UL1, UL2, and UL3*)

(1) Voltage waveform of the first phase line (UL1): The real data of UL1 and its amplitude are shown in Figs. 16(a) and (b) respectively. The LSTM output, for waveform prediction is shown in Fig. 16(c), indicating that the voltage waveform UL1 didn't contain any power quality events; therefore, this waveform is a normal voltage. The magnitude of this normal voltage computed from Fig. 16(b) is 0.97 p.u.

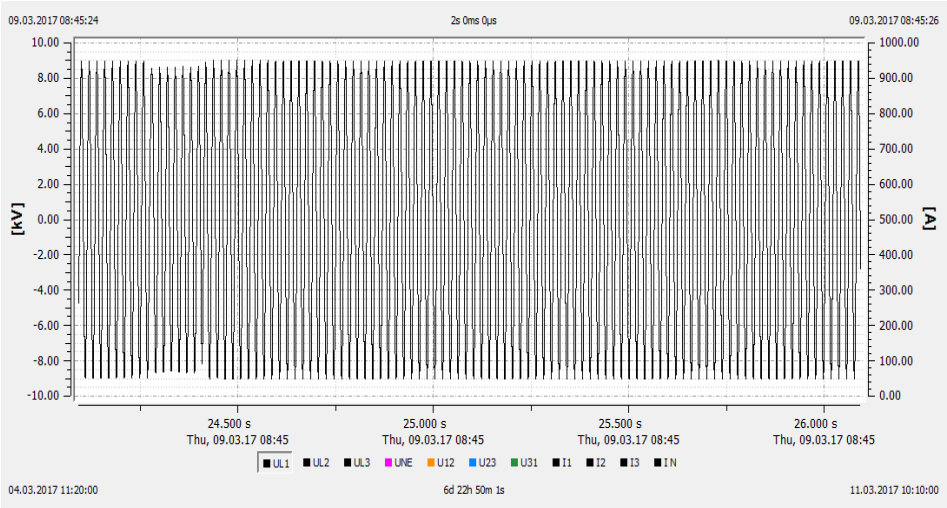

(a) Real waveform UL1

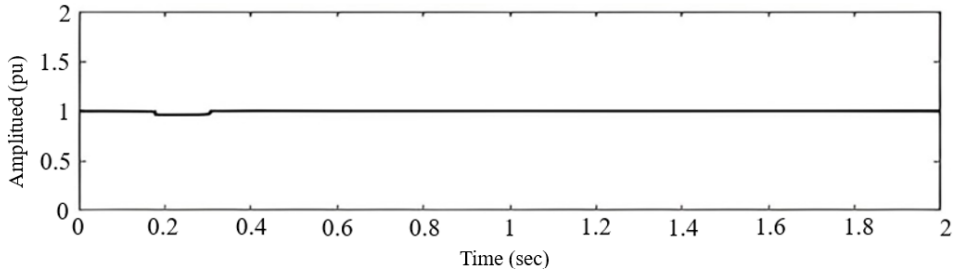

(b) Magnitude

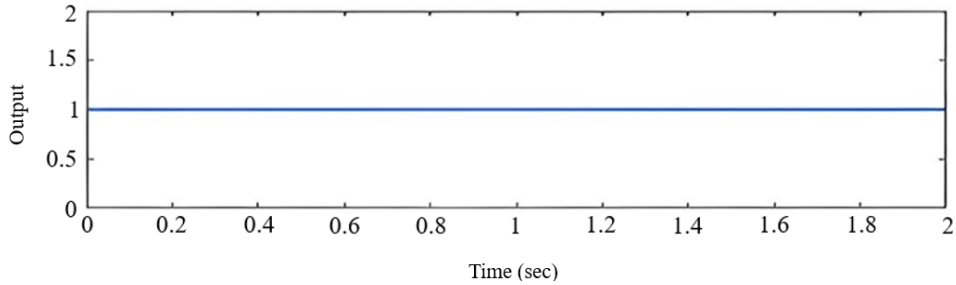

(c) LSTM output

Fig. 16 Recorded data 1 for UL1

(2) Voltage waveform of the second phase line (UL2): The real data of UL2, the prediction signal, and its amplitude are shown in Figs. 17(a), (b), and (c) respectively. The LSTM output is shown in Fig. 17(d), which indicates a PQ problem in waveform UL2: a voltage swell. The swell magnitude computed from Fig. 17(c), is 1.52 p.u. The start and end points of the swell are detected by using the LSTM output, as demonstrated in Fig. 17(d), the duration of the voltage swell is 158.2 ms.

(3) Voltage waveform of the third phase line (UL3): The real data of waveform UL3 and its amplitude are shown in Figs. 18(a) and (b) respectively. The LSTM output is shown in Fig. 18(c), which shows a power quality problem in voltage waveform UL3: a voltage sag. The amplitude of the voltage sag is computed from Fig. 18(b), which is 0.72 p.u. The start and end points of sag are detected by using the LSTM output, as presented in Fig. 18(c), the duration of voltage sag is 113.4 ms.

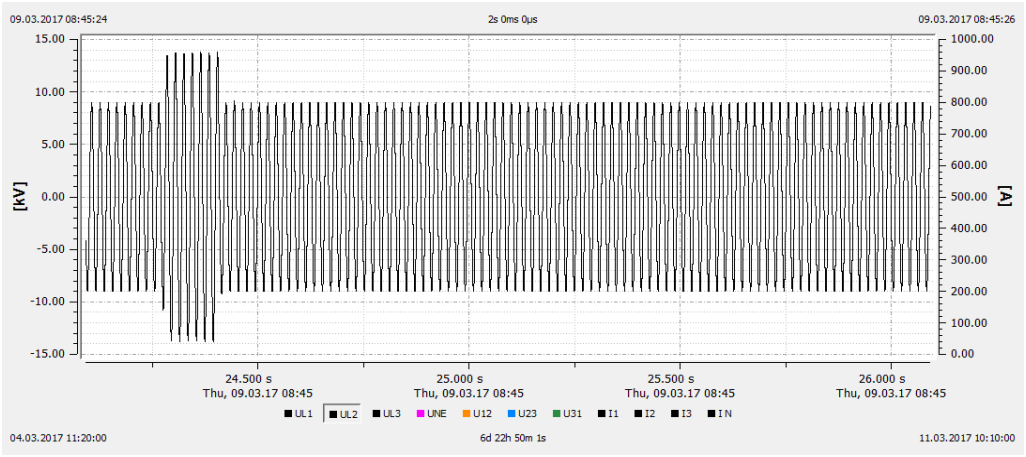

(a) Real waveform UL2

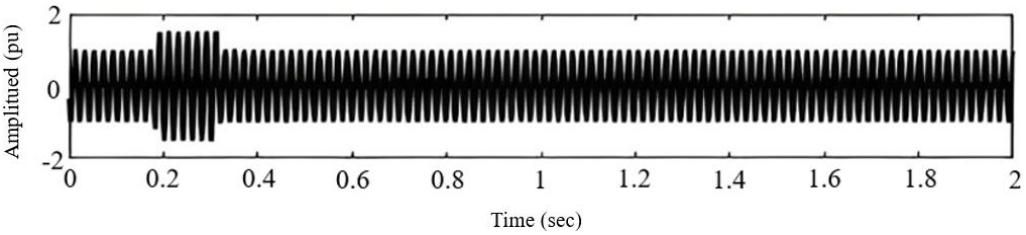

(b) Prediction waveform UL2

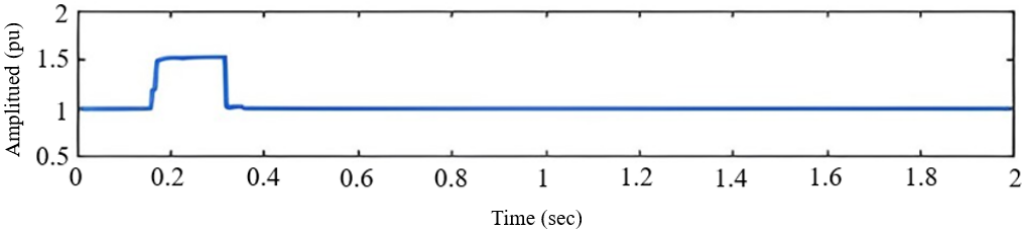

(c) Magnitude

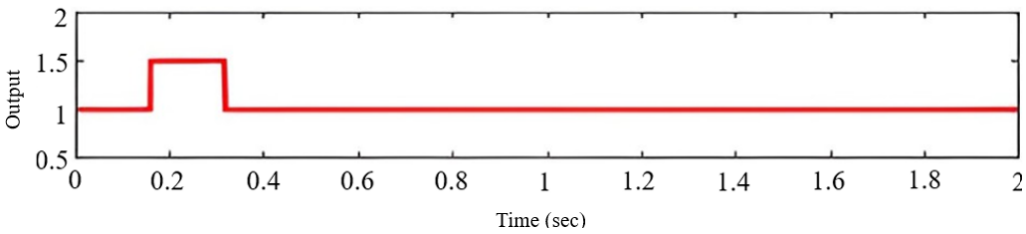

(d) LSTM output

Fig. 17 Recorded data 1 for UL2

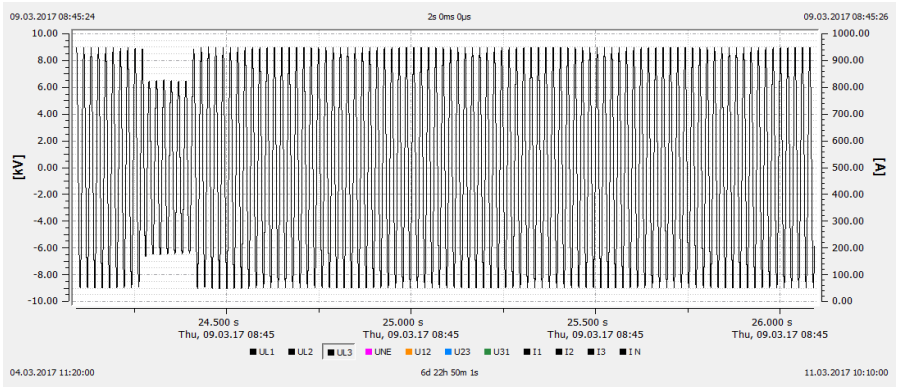

(a) Real signal UL3

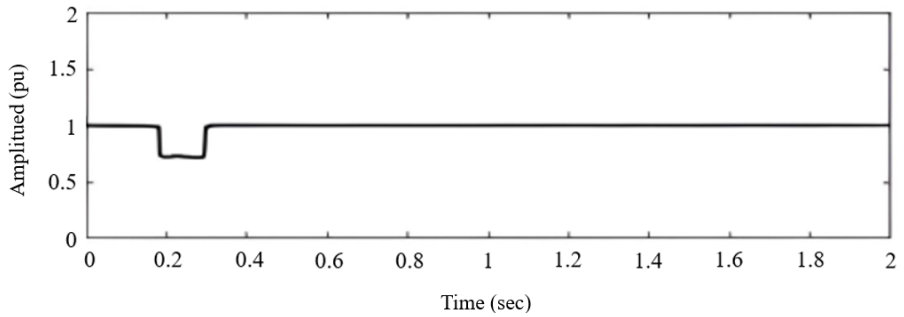

(b) Magnitude

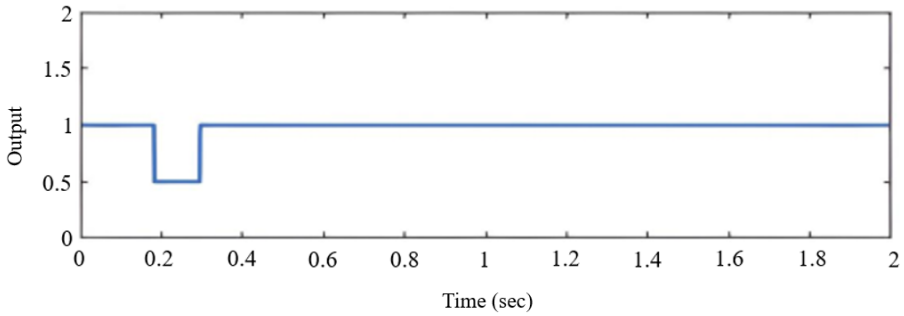

(c) LSTM output

Fig. 18 Recorded data 1 for UL3

5.7. Recorded data 2 (*the recorded data are for UL1*)

Voltage waveform UL1: The real data of voltage signal UL1 and its amplitude are shown in Figs. 19(a) and (b) respectively. The LSTM output is shown in Fig. 19(c), which demonstrates a PQ event in voltage waveform UL1: a voltage surge. The magnitude of the surge, as computed from Fig. 19(b) is 3.3 p.u.

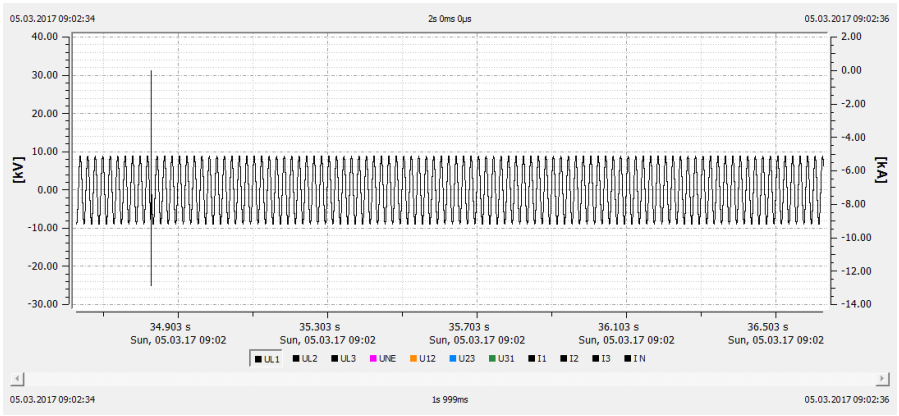

(a) Real signal UL1

Fig. 19 Recorded data 2 for UL1

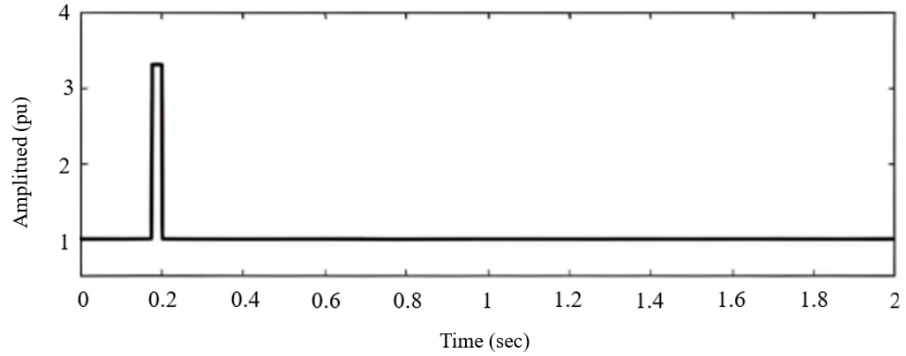

(b) Magnitude

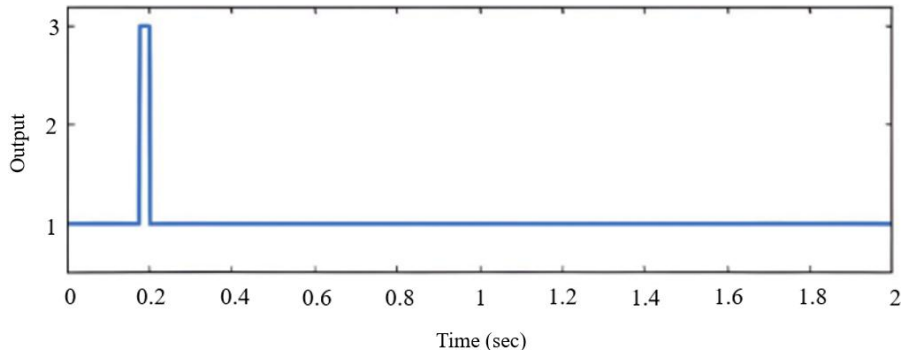

(c) LSTM output

Fig. 19 Recorded data 2 for UL1 (continued)

5.8. Recorded data 3 (*the recorded data are for UL1*)

Voltage waveform UL1: The real data of waveform UL1 and its amplitude are shown in Figs. 20(a) and (b) respectively. The LSTM output is shown in Fig. 20(c), which presents a PQ event in voltage waveform UL1: a voltage interruption. The magnitude of the voltage interruption, calculated from Fig. 20(b), is 0.0097 p.u. The start and end points of a voltage interruption are detected using the LSTM output, as shown in Fig. 20(c), the duration of voltage interruption is 1.8054 sec.

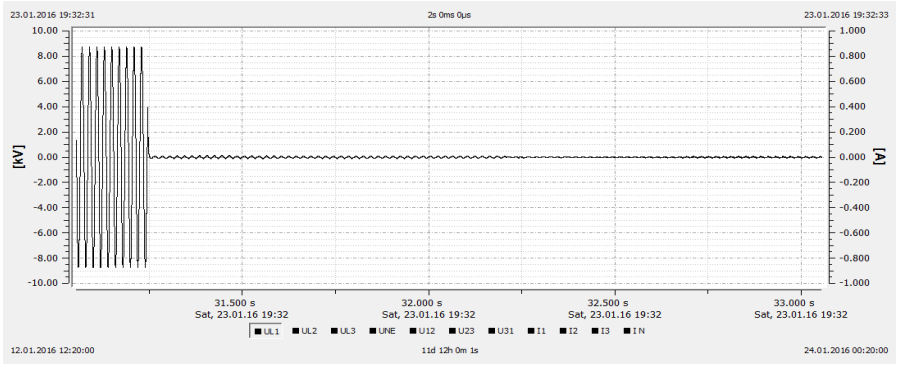

(a) Real signal UL1

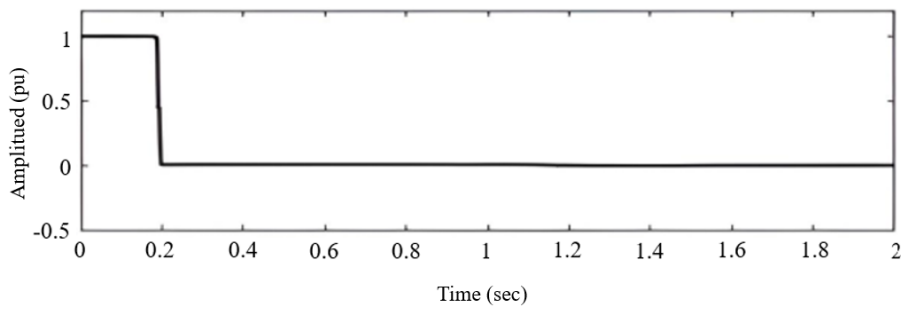

(b) Magnitude

Fig. 20 Recorded data 3 for UL1

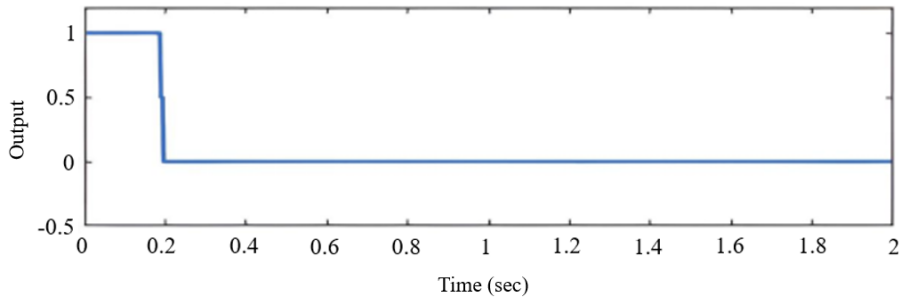

(c) LSTM output

Fig. 20 Recorded data 3 for UL1 (continued)

6. Conclusions

This study presents a significant application of a novel artificial intelligence (AI) technique to detect and identify power quality (PQ) problems such as interruptions, sags, swells, surges, flickers, and harmonic distortion. Several sets of real data (three-phase voltages and currents) are used to validate the effectiveness of the proposed technique in successfully identifying and detecting PQ problems. The real data, measured from an HV/MV substation, are recorded and analyzed using a data acquisition device. The proposed technique learns from and detects both simulated and real data based on three main components: advanced and automatic feature extraction, voltage/current magnitude computations, and PQ problem duration.

The projected technique, the long short-term memory (LSTM) network, which is a particular type of recurrent neural network (RNN), accomplishes classification accuracies of 100%, 94.56%, 98.22%, and 99.94% for noiseless and noisy conditions under signal-to-noise ratio (SNR) situations of 20 dB, 30 dB, and 40 dB, respectively. These results demonstrate superior efficiency compared to the Kalman filter (KF), feature extraction strategies (FES), short-time Fourier transform (STFT) with dynamics, adaptive linear neuron (ADALINE), feedforward neural networks (FFNN), and dynamic time warping (DTW) schemes. The simulation and real results propose that the LSTM technique is a favorable choice for future PQ analysis without the necessity for human experts, especially if larger datasets become accessible.

The outcomes of this study have important suggestions for both industry and academia. For industry, the proposed LSTM-based methodology offers a robust and scalable solution for real-time power quality monitoring and management, potentially reducing interruption and improving grid reliability. For academia, this work contributes to the growing body of knowledge on the application of deep learning techniques in electrical engineering, especially within the situation of smart grid technologies. Future studies will focus on covering the validation of the proposed LSTM model using more general real-world datasets from different topographical regions and power system configurations.

Additionally, there is a plan to investigate supplementary types of PQ disturbances and further optimize the model for real-time deployment in various environments. Moreover, the other aim is to explore hybrid approaches that integrate AI with traditional signal processing techniques to control the strengths of both methodologies for improved accuracy and robustness.

Conflicts of Interest

The authors declare no conflict of interest.

References

[1] N. Singh, M. A. Ansari, M. Tripathy, and V. P. Singh, “Feature Extraction and Classification Techniques for Power Quality Disturbances in Distributed Generation: A Review,” IETE Journal of Research, vol. 69, no. 6, pp. 3836-3851, 2023.

[2] D. H. Chiam, K. H. Lim, and K. H. Law, “LSTM Power Quality Disturbance Classification with Wavelets and Attention Mechanism,” Electrical Engineering, vol. 105, no. 1, pp. 259-266, 2023.

[3] P. Khetarpal, N. Nagpal, P. Siano, and M. Al-Numay, "Power Quality Disturbance Signal Segmentation and Classification Based on Modified BI-LSTM with Double Attention Mechanism," IET Generation, Transmission & Distribution, vol. 18, no. 1, pp. 50-62, 2024.

[4] S. Cen, D. O. Kim, and C. G. Lim, "A Fused CNN-LSTM Model Using FFT with Application to Real-Time Power Quality Disturbances Recognition," Energy Science & Engineering, vol. 11, no. 7, pp. 2267-2280, 2023.

[5] I. S. Samanta, S. Panda, P. K. Rout, M. Bajaj, M. Piecha, V. Blazek, et al., "A Comprehensive Review of Deep-Learning Applications to Power Quality Analysis," Energies, vol. 16, no. 11, article no. 4406, 2023.

[6] X. Y. Zheng, C. P. Chen, and J. A. Jiang, "An Embedded-Based Distributed Private Cloud: Power Quality Event Classification," Proceedings of IEEE International Conference on High Performance Computing and Communications, pp. 1237-1242, 2014.

[7] O. P. Mahela and A. G. Shaik, "Recognition of Power Quality Disturbances Using S-Transform and Rule-Based Decision Tree," Proceedings of IEEE 1st International Conference on Power Electronics, Intelligent Control and Energy Systems, pp. 1-6, 2016.

[8] P. K. A. Kumar, V. J. Vijayalakshmi, J. Karpagam, and C. K. Hemapriya, "Classification of Power Quality Events Using Support Vector Machine and S-Transform," Proceedings of 2nd International Conference on Contemporary Computing and Informatics, pp. 279-284, 2016.

[9] S. Alshahrani, M. Abbod, and G. Taylor, "Detection and Classification of Power Quality Disturbances Based on Hilbert-Huang Transform and Feed Forward Neural Networks," Proceedings of 51st International Universities Power Engineering Conference, pp. 1-6, 2016.

[10] T. A. Kawady, N. I. Elkalashy, A. E. Ibrahim, and A. M. I. Taalab, "Arcing Fault Identification Using Combined Gabor Transform-Neural Network for Transmission Lines," International Journal of Electrical Power & Energy Systems, vol. 61, pp. 248-258, 2014.

[11] N. Köse, Ö. Salor, and K. Leblebicioğlu, "Interharmonics Analysis of Power Signals with Fundamental Frequency Deviation Using Kalman Filtering," Electric Power Systems Research, vol. 80, no. 9, pp. 1145-1153, 2010.

[12] A. A. Abdelsalam, A. A. Eldesouky, and A. A. Sallam, "Classification of Power System Disturbances Using Linear Kalman Filter and Fuzzy-Expert System," International Journal of Electrical Power & Energy Systems, vol. 43, no. 1, pp. 688-695, 2012

[13] P. C. Chang, G. W. Chang, M. H. Shih, Y. Y. Chen, Y. H. Hong, and Y. K. Yeh, "A Hybrid Approach for Detection and Classification of Power Quality Disturbances," Proceedings of IEEE Power & Energy Society General Meeting, pp. 1-5, 2017.

[14] F. Hafiz, S. Abecrombie, A. Eaton, C. Naik, and A. Swain, "Power Quality Event Identification Using Wavelet Packet Transform: A Comprehensive Investigation," Proceedings of IEEE Region 10 Conference, pp. 2978-2983, 2017.

[15] M. H. Ali, A. S. Kaittan, and M. S. Ibrahim, "Design and Deployment of a Voice Activated for Intelligent Robot," E3S Web of Conferences, vol. 474, article no. 02007, 2024.

[16] J. Y. Ren, J. W. Zhao, N. Pan, N. B. Zhang, and J. W. Yang, "Prediction of Distribution Network Line Loss Rate Based on Ensemble Learning," International Journal of Engineering and Technology Innovation, vol. 14, no. 1, pp. 103-114, 2024.

[17] A. I. Jaber, A. S. Kaittan, M. W. Abdulwahhab, and D. V. Samokhvalov, "Efficiency Improvement of PM Synchronous Wind Generator Using Field Oriented Control with Model-Base Current Observer," International Review of Electrical Engineering, vol. 19, no. 1, pp. 22-30, 2024.

[18] O. Ozupek, R. Yilmaz, B. Ghasemkhani, D. Birant, and R. A. Kut, "A Novel Hybrid Model (EMD-TI-LSTM) for Enhanced Financial Forecasting with Machine Learning," Mathematics, vol. 12, no. 17, article no. 2794, 2024.

[19] Y. Jiang, P. Dai, P. Fang, R. Y. Zhong, X. Zhao, X. Cao, et al., "A 2-LSTM for Predictive Maintenance of Industrial Equipment Based on Machine Learning," Computers & Industrial Engineering, vol. 172, no. PA, article no. 108560, 2022.

[20] L. Zhang, X. Zhu, S. Zhao, and D. Xu, "A Novel Virtual Network Fault Diagnosis Method Based on Long Short-Term Memory Neural Networks," Proceedings of IEEE 86th Vehicular Technology Conference, pp. 1-5, 2017.

[21] I. S. Samanta, S. Panda, P. K. Rout, M. Bajaj, M. Piecha, V. Blazek, et al., "A Comprehensive Review of Deep-Learning Applications to Power Quality Analysis," Energies, vol. 16, no. 11, article no. 4406, 2023.

[22] A. Kumar and M. N. Alam, "Bidirectional LSTM Network-Based Short-Term Load Forecasting Method in Smart Grids," Proceedings of 5th International Conference on Energy, Power and Environment: Towards Flexible Green Energy Technologies, pp. 1-6, 2023.

[23] L. Kirichenko, Y. Koval, S. Yakovlev, and D. Chumachenko, "Anomaly Detection in Fractal Time Series with LSTM Autoencoders," Mathematics, vol. 12, no. 19, article no. 3079, 2024.

[24] O. P. Mahela and A. G. Shaik, "Recognition of Power Quality Disturbances Using S-Transform Based Ruled Decision Tree and Fuzzy C-Means Clustering Classifiers," Applied Soft Computing, vol. 59, pp. 243-257, 2017.

[25] R. Kumar, B. Singh, and D. T. Shahani, "Symmetrical Components-Based Modified Technique for Power-Quality Disturbances Detection and Classification," IEEE Transactions on Industry Applications, vol. 52, no. 4, pp. 3443-3450, 2016.

[26] M. Valtierra-Rodriguez, R. Romero-Troncoso, R. A. Osornio-Rios, and A. Garcia-Perez, "Detection and Classification of Single and Combined Power Quality Disturbances Using Neural Networks," IEEE Transactions on Industrial Electronics, vol. 61, no. 5, pp. 2473-2482, 2014.

[27] M. Biswal and P. K. Dash, "Measurement and Classification of Simultaneous Power Signal Patterns with an S-Transform Variant and Fuzzy Decision Tree," IEEE Transactions on Industrial Informatics, vol. 9, no. 4, pp. 1819-1827, 2013.

[28] S. He, K. Li, and M. Zhang, "A Real-Time Power Quality Disturbances Classification Using Hybrid Method Based on S-Transform and Dynamics," IEEE Transactions on Instrumentation and Measurement, vol. 62, no. 9, pp. 2465-2475, 2013.

[29] J. Li, Z. Teng, Q. Tang, and J. Song, "Detection and Classification of Power Quality Disturbances Using Double Resolution S-Transform and DAG-SVMs," IEEE Transactions on Instrumentation and Measurement, vol. 65, no. 10, pp. 2302-2312, 2016.

[30] M. S. Manikandan, S. R. Samantaray, and I. Kamwa, "Detection and Classification of Power Quality Disturbances Using Sparse Signal Decomposition on Hybrid Dictionaries," IEEE Transactions on Instrumentation and Measurement, vol. 64, no. 1, pp. 27-38, 2015.

Copyright© by the authors. Licensee TAETI, Taiwan. This article is an open access article distributed under the terms and conditions of the Creative Commons Attribution (CC BY-NC) license (http://creativecommons.org/licenses/by/4.0/).